Hybrid quantum simulations of biomolecules: the role of copper in neurodegenerative diseases

J. Bernholc,[1] M. Hodak, W. Lu, and F. Rose

[1]Center for High Performance Simulation and Department of Physics
North Carolina State University
Raleigh, North Carolina, 27695

E-mail: bernholc@ncsu.edu

Abstract. One of the most important challenges in quantum simulations of biomolecules is efficient and accurate inclusion of the solvent, because the solvent atoms usually far outnumber those of the solute. We have developed a hybrid method that allows for explicit quantum-mechanical treatment of the solvent at low computational cost. It combines Kohn-Sham (KS) density functional theory (DFT) with fixed-density orbital-free (FDOF) DFT. KS DFT is used to describe the biomolecule and its first solvation shells, while the FDOF DFT is employed for the rest of the solvent. The FDOF method scales linearly with the number of atoms and is capable of handling 10^5 solvent molecules on current supercomputers, while taking only a small percentage of the total computational time. The compatibility between the KS and OF DFT methods enables seamless integration between the two. In particular, the flow of solvent molecules across the KS/FDOF interface is allowed and the total energy is conserved. The hybrid method has been used to investigate the binding of copper ions to the prion protein (PrP), which is responsible for a group of neurodegenerative diseases called the transmissible spongiform encephalopathies, such as Cruetzfeldt-Jakob in humans or mad cow disease in cattle. Our results show that as copper ions successively bind to the PrP, the protein changes its shape to accommodate the ions. The binding sequence is such that while the binding energy per copper ion decreases, the energy balance is still positive and up to four copper ions can be bound. PrP acts thus as a copper buffer. Furthermore, the copper-bound PrP becomes more stable and more resistant to misfolding. Therefore, copper plays a beneficial role in the initial stages of prion diseases.

1. Introduction

Accurate representation of solvation is one of the most important aspects of simulations on biomolecules. The solvent not only determines the shape of biomolecules, but it also plays a direct role in many biological processes. The difficulty of dealing with solvation stems from the fact that a large number of solvent molecules is required in a simulated system and the solvent atoms usually outnumber those of the the solute, which are of main interest.

The computational cost of treating the solvent is particularly important for quantum simulations, where systems of ~10^3 atoms can be treated at present and the cost of the simulation increases dramatically with the number of atoms. For that reason, there is substantial interest in developing methods for efficient description of solvation effects. One way is to use implicit representation of the solvent. In such methods, the solvent is represented as a polarizable continuum dielectric [1,2,3]. These methods are highly efficient, since they eliminate the need for direct treatment of the solvent

molecules. This approach was successfully used [4,5,6,7] in many instances, but evidence suggests that for full understanding of the behavior of many biological systems an explicit treatment is essential. For example, molecular mechanics simulations of proteins have shown that an implicit representation leads to incorrect predictions of native structures and folding pathways, while explicit treatment of the solvent yields results in agreement with experimental observations [8,9]. Furthermore, for many solvated biomolecules water molecules are located near the active sites and are essential to their functions. To properly describe these water molecules, hydrogen bonds with other water molecules have to be included and this can only be done when the solvent is treated explicitly.

Explicit representation of full solvation in quantum calculations is only feasible when the solvent molecules are represented in a simplified manner at a lower level of theory than the solute. A typical example of this approach is the QM/MM method [10,11,12], which combines ab initio and molecular mechanics simulations. In QM/MM, the chemically active part of the system is treated at an ab initio level, while the rest of the system, including the solvent and remainder of the solute, is treated with classical force fields methods. The weak point of QM/MM schemes is the treatment of interaction between the QM and MM subsystems. A special energy term is required to describe this interaction. It usually employs force field parameters, which were developed and tested in calculations within classical molecular mechanics and not for interactions between the QM and MM subsystems. Furthermore, to allow for the flow of solvent molecules across the QM/MM interface, resulting in exchange of molecules between the subsystems, buffer regions and force smoothing functions have to be used [13].

We have recently developed [14] a different approach to hybrid simulations, in which two density functional methods are combined. The chemically active part of the system is treated with the usual ab initio Kohn-Sham DFT, while a frozen-density orbital-free (FDOF) DFT method, which scales linearly with the number of atoms, is used for the rest of the system. In this method, the solvent molecules are assumed to have rigid geometries and frozen electron densities. The advantage of combining two DFT methods is that interactions between the subsystems can be treated at the quantum level rather than at the level of molecular mechanics, as is usually the case in QM/MM methods. In addition, the KS/FDOF method provides seamless integration between the subsystems and allows for the flow of the molecules across the KS/FDOF interface without the need for a buffer region or force smoothing. Within the KS/FDOF method, energy conserving molecular dynamics simulations can be run even when molecules are exchanged between the subsystems.

As an initial application, this method was used [15] to study interactions of copper ions with the prion protein (PrP). PrP is responsible or a group of neurodegenerative diseases called transmissible spongiform encephalopathies (TSEs) [16,17]. The TSEs include bovine spongiform encephalopathy or "mad cow disease" in cattle, scrapie in sheep, chronic wasting disease in deer and elk, kuru and Creutzfeldt-Jakob disease in humans. The PrP structure is characterized by a folded, mostly α-helical, C-terminal domain and an unfolded, flexible, N-terminal region. In TSEs, the prion protein misfolds and aggregates into amyloidic deposits. The detailed structure of the misfolded PrP has not been resolved yet, but it is known that the deposits are β-sheet rich [18]. The normal function of the PrP^C in healthy tissue is still unknown. However, it is now well established [19,20] that the PrP^C efficiently binds Cu^{2+} and further studies [21] link this ability to its function.

To better understand the copper-related function of PrP, copper attachment to PrP has to be fully elucidated. To this end, we use the KS/FDOF hybrid method to study interactions between copper and PrP in various binding modes, which have been suggested experimentally [22]. In particular, we calculate for the first time the attachment geometries and binding energies for low and medium copper concentration conditions. Our analysis of the energetics shows that PrP is capable of carrying out copper buffering function as previously suggested [23]. Starting from these copper-attachment geometries, we perform molecular mechanics simulations of the full length PrPC. These reveal that binding of copper leads to development of new structural features in the unfolded part of the protein increasing the stability of the entire copper-coordinating region. Since the stabilized protein has a

lesser tendency to misfold, this result suggests a protective role of copper in the initial stages of prion diseases.

2. Hybrid Kohn-Sham DFT/Frozen-Density Orbital-Free DFT Method

Within KS/FDOF DFT, the solvent molecules are described with a frozen-density orbital-free (FDOF) DFT method. These molecules are assumed to have rigid geometries and frozen electron densities. The combined total energy is given by the following expression:

$$E_{FDOF}[\varrho] = T_{OF}[\varrho] + E_H[\varrho] + E_{XC}[\varrho] + E_{PPlocal}[\varrho] + E_{AA} \tag{1}$$

where T_{OF} stands for the orbital-free (*OF*) kinetic energy (*KE*) functional, E_H is the Hartree energy, E_{XC} is the exchange correlation energy, $E_{PPlocal}$ evaluates the energy of interaction between the electrons and the local part of the pseudopotentials, and E_{AA} denotes the interaction energy between the atomic cores in the system. Any *OF KE* functional can be used in the formula above, but we have found that the LLP [24] functional works well in calculations for liquid water:

$$T_{LLP} = C_{TF} \int_{\Omega} \varrho^{5/3} \left(1 + \frac{0.0045x^2}{1 + 0.0253x \sinh^{-1} x} \right) d\mathbf{r}, \tag{2}$$

where

$$x = 2^{1/3} \frac{|\nabla \varrho(\mathbf{r})|}{\varrho^{4/3}(\mathbf{r})}. \tag{3}$$

Note that only the local part of the pseudopotential is used in Eq. 1, the reason being that the non-local part of pseudopotential is applied to orbitals rather than the charge density. Neglecting the non-local contributions is well justified, because the present method only deals with intermolecular interactions (molecules are assumed to have frozen geometries and charge densities), and the short-range non-local effects are negligible at typical intermolecular distances.

For expediency, the charge density for each solvent molecule is described by gaussians centered on ionic positions. The coefficients are adjusted so that the charge and the dipole moment of the water molecule are correctly reproduced. The obtained radial distribution functions (RDFs) of this simple model compare well to experimental results for liquid water, as shown in Figure 1.

To define a hybrid calculation scheme combining the FDOF and KS methods, consider a system that contains two types of atoms: those that are treated with the FDOF method (FDOF atoms) and those that are treated with the KS DFT method (KS atoms). The FDOF atoms have fixed charge densities attached to them, which sum up to $\varrho_{FDOF}(\mathbf{r})$, while the charge density corresponding to the KS atoms, $\varrho_{KS}(\mathbf{r})$, minimizes the energy functional for the hybrid system. The total charge density of the entire system is simply the sum of both densities

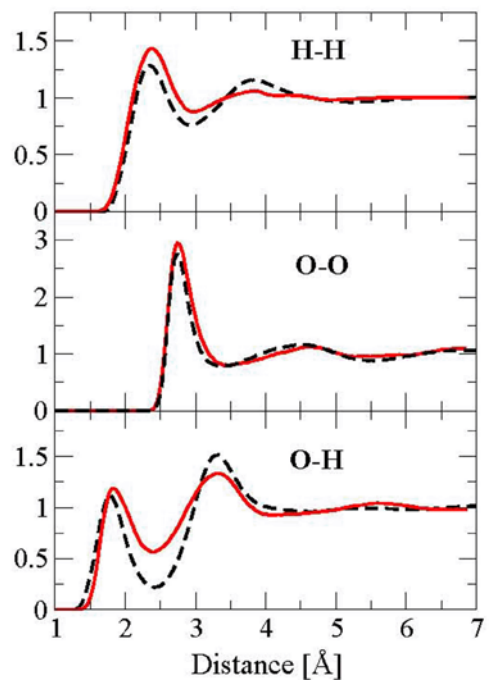

Figure 1. Radial distribution functions calculated using the frozen-density method (solid lines) for a system of 432 water molecules at 300 K. Experimental results [25] are also shown (dashed lines). For better comparison, intramolecular features in H-H and O-H plots were removed from the experimental data.

$$\varrho_{tot} = \varrho_{FDOF} + \varrho_{KS}. \tag{4}$$

Since the Hartree and exchange-correlation energies are explicit functions of the charge density, it is straightforward to calculate these quantities for the hybrid system using ϱ_{tot}. The atom-atom interaction energy is also straightforward, being the sum over all atoms present in the hybrid system, regardless of their type. As for as the pseudopotential energy, the local and non-local parts are treated differently: each atom has a local potential associated with it and it acts on the total density ϱ_{tot}, while only the KS atoms have non-local potentials associated with them and these only act on the KS orbitals.

Defining KE of the hybrid system is somewhat more complicated. Taking the sum of the FDOF and KS KEs is not sufficient, since kinetic energies are non-additive. The non-additive part of KE can be estimated [26] as

$$T_{nadd}[\varrho_{FDOF}, \varrho_{KS}] = T_{OF}[\varrho_{tot}] - T_{OF}[\varrho_{FDOF}] - T_{OF}[\varrho_{KS}]. \tag{5}$$

This gives the following functional for the total electron energy of a hybrid system:

$$\begin{aligned} E_{Hybrid}[\varrho_{FDOF}, \varrho_{KS}, \{\mathbf{R}_i\}_{FDOF}, \{\mathbf{R}_i\}_{KS}] = \quad & T_{TF}[\varrho_{TF}] + T_{KS}[\varrho_{KS}] + T_{nadd}[\varrho_{FDOF}, \varrho_{KS}] \\ + \quad & E_H[\varrho_{tot}] + E_{XC}[\varrho_{tot}] + E_{PP_{nonloc}}[\varrho_{KS}, \{\mathbf{R}_i\}_{KS}] \\ + \quad & E_{PP_{loc}}[\varrho_{tot}, \{\mathbf{R}_i\}] + E_{AA}[\{\mathbf{R}_i\}]. \end{aligned} \tag{6}$$

Here $\{\mathbf{R}_i\}$ denotes all atoms in the system and $\{\mathbf{R}_i\}_{KS}$ stands for atoms treated by the KS DFT. Note that in this functional ϱ_{FDOF} is rigidly tied to the positions of FDOF atoms, while ϱ_{KS} is determined by minimizing the energy functional above.

An important feature of our method is that it allows for for the flow of molecules across the interface between the regions treated by the different methods. Being able to deal with a change in the number of KS atoms is important, since in dynamical calculations the number of solvent molecules in first solvation shells or within the KS region can change. It is also possible that a solvent molecule originally treated by the KS method moves out of the KS region. Such molecule cannot be treated by the KS DFT anymore, since it is required that all KS atoms are inside the KS region, and the number of KS atoms has to be decreased. When such an event occurs, the KS/FDOF simulation can readily continue, since the total electron energy in KS/FDOF system (Eq. 6) can be calculated for any number of KS and FDOF molecules. However, the exchange causes discontinuities in the total electron energy, due to the fact that the electron energy of a solvent molecule is different when calculated with KS or FDOF methods. Nevertheless, these discontinuities can be simply removed by subtracting differences in total energy before and after each exchange. This procedure yields an essentially constant total energy and smooth kinetic energy curves as a function of simulation time, thus enabling energy-conserving quantum molecular dynamics simulations.

3. Copper-PrP Interaction

As an initial application of the KS/FDOF technique, the binding of copper ion to the prion protein, PrP, is investigated. The PrP is implicated in a group of neurodegenerative diseases called transmissible spongiform encephalopathies. These include bovine spongiform encephalopathy (BSE) or “mad cow disease” and the Creutzfeldt-Jakob disease (CJD). The physiological function of the PrP is unknown, but recent investigations [27,28,21,29,30,31] suggest that it may be linked to its ability to bind copper.

A range of experimental techniques, including EPR [32,33,34], CD [35], X-ray crystallography [36] and NMR [37,38] have been used to investigate Cu^{2+} binding to PrP. These studies determined that, at maximum copper occupancy, the full-length prion protein can bind five or six copper ions. Four of these binding sites are located in the octarepeat domain, residues 60-91, which consists of four tandem repeats of the aminoacid sequence PHGGGWGQ. In this case the copper ions are coordinated by a single histidine residue, deprotonated backbone amide nitrogens, and a backbone carboxyl

oxygen. This mode of binding has been confirmed by theoretical studies [14,39] and the copper geometry is displayed in Figure 2.

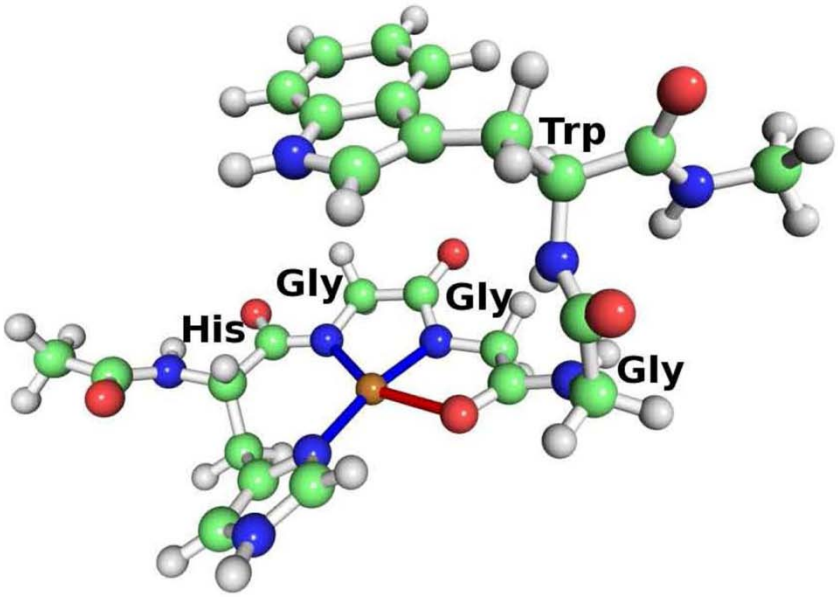

Figure 2. Binding of copper ion to a HGGGW fragment. The copper ion is shown in gold, carbon atoms are colored green, nitrogen atoms blue, oxygen atoms red and hydrogens light grey.

More recent experimental works have found that this picture of copper attachment to the octarepeat domain is incomplete and that different modes of attachment occur depending on environmental factors. EPR investigation by Chattopadhyay et al. [22] demonstrated that copper attachment to the octarepeat region of the prion protein depends on its concentration and that the 1:1 attachment, denoted as Component 1 [22], only takes place at high concentrations. When copper concentration decreases two other coordination modes occur. At low concentration, one copper ion is coordinated by either three or four histidines from different repeats. The exact number of histidines participating in this binding, called Component 3, could not be determined. Interestingly, the same type of binding could be obtained by decreasing pH of the solution [40]. The reason for this is that at low pH, deprotonation of amide nitrogens, which is needed to establish Component 1 binding, becomes unfavorable. The copper ion is thus coordinated by histidine residues instead. At intermediate concentrations, the copper can coordinate to one or two histidines, two water molecules, and a deprotonated backbone nitrogen.

Hybrid KS/FDOF calculations have been used [15] to map out these stages of copper binding. In these calculations, the prion protein was represented by fragments of binding residues to which neutral ends were applied. The fragments, the copper ion and the water molecules closest to the copper ion (6–9 water molecules, depending on the type of binding) were treated by the full Kohn-Sham (KS) DFT. The remainder of the simulation cell was filled with water molecules at liquid density. The water molecules not included in the KS DFT are treated by the orbital-free DFT.

The low concentration binding mode was investigated first. For this type of copper attachment, the experiments found that the copper ion is coordinated by multiple imidazole groups of histidine residues. However, their exact number (three or four) could not be determined. Our calculations consider both these possibilities. Since imidazoles have two nitrogen atoms capable of coordinating metals, commonly denoted as N_δ and N_ε, attachments involving both these nitrogens were investigated for each case. The results show that coordination of the copper ion by four histidine residues through

N_ε atoms is the most favorable energetically. The binding is predominantly planar, with copper-coordinating nitrogens arranged in a slightly distorted square, see Figure 3.

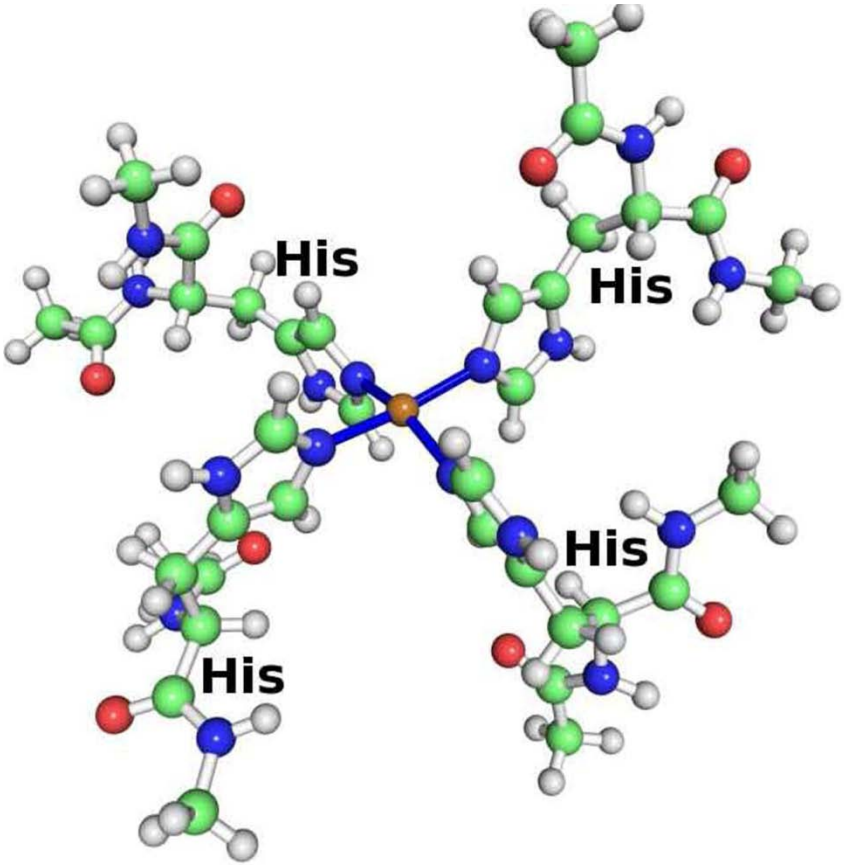

Figure 3. The structure of the low concentration copper binding site in the octarepeat domain of PrP.

For moderate concentration of copper, experiments [22] indicate the involvement of two histidine imidazoles, along in the equatorial and axial positions, although the presence of the axial histidine could not be conclusively proven. Our calculations confirm the presence of axial histidine residues and also show the involvement of two water molecules in the equatorial plane. The obtained binding structure is shown in Figure 4.

4. PrP as a Copper Buffer

One of the most important open questions in PrP research is the normal function of PrP in healthy tissues. After misfolding, it loses the ability to perform this function, which undoubtedly is an important factor in the disease. In fact, several lines of research point to a neuroprotective role of PrP in the brain. For example, comparison between normal and PrP knockout mice shows [41] that the knockout mice have extensive oxidative damage not present in the normal one. Furthermore, neurons containing PrP are more resistant to copper toxicity than cells lacking the protein [27,42,43]. At present, the leading hypothesis for PrP's function in vivo is that it acts as a copper buffer [23], binding uncomplexed extracellular Cu^{2+} and protecting other proteins from its deleterious effects. Using insights from these the copper binding calculations presented above, we now analyze the plausibility of the copper buffer hypothesis.

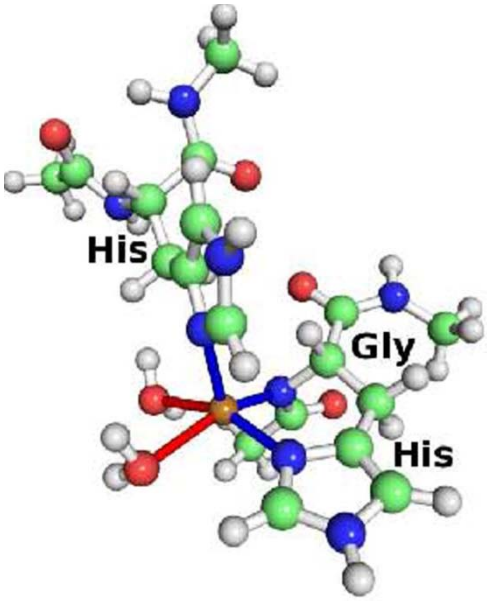

Figure 4. The structure of the medium concentration copper binding mode in the octarepeat domain of PrP.

For each of the three binding modes, we calculate the binding energies of Cu^{2+} to PrP^{C} relative to Cu^{2+} solvated in water. The low concentration, multiple-histidine binding has the energy of 5.22 eV, which is the largest. The medium concentration coordination of copper is less strong, with a binding energy of 2.75 eV. The high occupancy, high concentration binding is the weakest, with an energy gain of 1.76 eV. These results are consistent with recent experimental values for PrP^{C}'s copper affinity [44,45], where the same ordering was found, with low concentration binding being in the nanomolar range, while the high coordination concentration reached micromoles.

For the buffering function of PrP, it is important to consider the number of copper ions that can be coordinated in each of the modes, in addition to the strength of each individual mode. In the low concentration mode, only one copper ion can be coordinated, since all four of the histidine residues in the octarepeat domain participate in its binding. The medium concentration binding mode requires two histidine residues and thus two copper ions can be bound. Finally, four copper ions can be bound to the octarepeat region in the high concentration binding mode, which only requires one histidine residue per each copper ion. The high number of copper ions that can be bound in the high concentration mode means that it is the most energetically favorable overall, even though it is the weakest type of attachment. The energy of 7.04 eV (4 × 1.76 eV) can be gained when four copper ions are bound in this mode. Other binding modes provide smaller energy gains when fully occupied, see Table 1. Note that the binding energy gain increases with copper concentration, confirming that the PrP can act as a copper buffer, since it is energetically favorable to bind more copper ions when they are available in the environment.

Table 1. Energies of copper binding modes for octarepeat domain of PrP

Building mode	Binding energy (eV)	Number of bound ions	Total binding energy (eV)	Free energy change at 300 K (eV)
High concentration	1.76	4	7.04	–2.21
Medium concentration	2.75	2	5.50	–0.44
Low concentration	5.22	1	5.22	0

These results hold true even when the free energies are calculated, because the entropy of the Cu-containing PrP increases when the number of Cu ions bound to PrP increases. This is because the attachment of a single Cu ion, while having the largest binding energy, imposes severe constraints on the internal degrees of freedom of the PrP, bonding to four histidine residues in the octarepeat region. In the intermediate binding mode, only two histidine residues are coordinated to each Cu ion, allowing for increased thermal motion, while in the high concentration case each Cu ion binds to a single residue, leaving the PrP even less constrained. This qualitative argument is confirmed by our classical molecular dynamics simulations on full-length models for all three modes of Cu-bound PrP and calculating entropies using Schlitter's method [46,47]. The results are listed in the last column of 1.

5. Role of Copper in Prion Diseases

In addition to studying local binding geometry of the copper-PrP complex, we also investigate structural properties of full-length copper-bound proteins. The structure of free PrP was also investigated, so that the effect of copper can be determined. Molecular mechanics, as implemented in NAMD [48] is used in this study, due to the large number of atoms required in the simulations. Since the N-terminal domain of PrP^C is unfolded and flexible, the structure of full-length PrP cannot be revealed by current experiments. Even with the use of computer simulation, determining the structure of the full-length PrP^C is challenging, since no experimental data can be used to form an initial structure. Furthermore, because the N-terminal domain is unfolded, even the equilibrium structure is highly flexible, instead of being well defined as in the case of folded proteins. In addition, the unfolded part of the PrP^C takes up significantly more space than a folded protein of the same size and therefore requires a substantially larger simulation cell than a typical folded protein with the same number of residues. To overcome these difficulties, a massively parallel, long-time simulation is used to explore the structural properties of full-length PrP^C.

Snapshots of full-length free and copper bound PrP are shown in Figure 5. Note that the octarepeat region (shown in blue in the Figure 5) has to undergo significant restructuring in order to accommodate all of the binding modes. Such structural flexibility would not be possible for a fully folded protein. Therefore, the flexible character of the N-terminal domain is important, since it allows the PrP to perform its function.

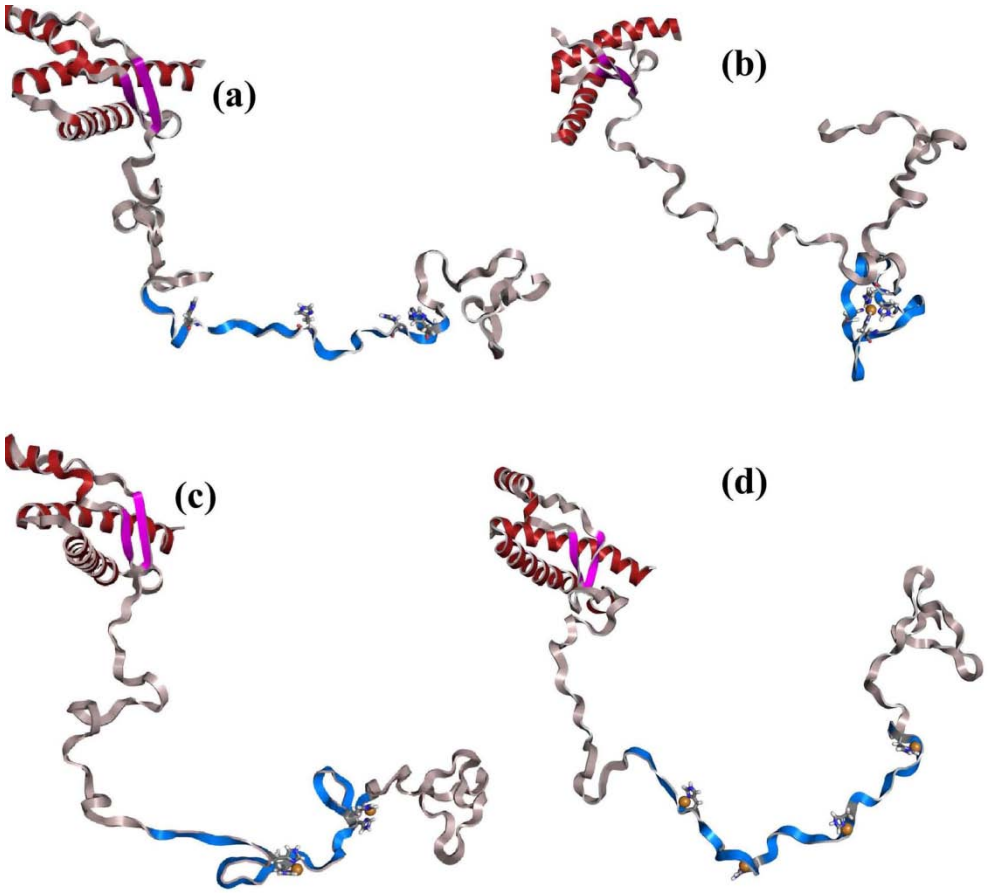

Figure 5. Structures of full-length prion protein in various copper binding modes. (a) Free PrP, (b) Low concentration mode, 1 copper ion attached, (c) medium concentration mode, 2 copper ions attached, (d) high concentration mode, 4 copper ions attached. The octarepeat domain is colored blue.

Since the low concentration binding mode is likely the most physiologically relevant, due to its copper affinity, which is similar to that of other copper-binding proteins [44,49,50], we investigate its structural properties in further detail. A snapshot of its structure is shown in Figure 5b. The binding of copper causes formation of three turns in the intermediate PrP segments connecting the binding histidine residues. Outside of the copper binding domain, the flexible part of the protein behaves in a fashion similar to the free PrP.

Importantly, the simulations also show stiffening of the flexible N-terminal domain upon binding of the copper ion; the unstable structural features formed in the N-terminal domain of PrP persist on average 17% longer in copper-bound PrP, compared to the free PrP. This implies a positive role of copper in the initial stages of prion diseases, since copper-bound PrP is harder to misfold due to stiffening of its structure.

Interestingly, protective effect of copper binding to PrP was also suggested in another computational study performed by Cox et al. [51], even though it considered binding at a different binding site located at His96. This study found that backbone bending at that site is incompatible with the proposed models of misfolded PrP [52,53], thus suggesting a protective role of copper attachment.

6. Summary and Conclusions

Thy hybrid KS/FDOF method provides an effective way for including explicit solvent in quantum biosimulations at low computational cost. In this approach the biomolecule, or its fragment, and solvent molecules in the first solvation shells are treated by full Kohn-Sham DFT, while the remaining solvent molecules are expeditiously described using frozen-density, orbital-free DFT. This method allows for efficient and accurate description of solvent effects and provides seamless integration between regions treated by the KS and FDOF DFT methods.

A first application to multistage copper binding to PrP was also presented. We determined the geometries and binding energies of the low, medium and high concentration modes. The results show that as the number of available copper ions increases, the binding site(s) will spontaneously rearrange to accommodate more copper ions with a net energy gain, despite the fact that the binding strength per copper ion decreases with the number of ions per PrP. The strong affinity for Cu and the multiplicity of concentration-dependent copper binding sites strongly supports the previously suggested copper buffering role of the prion protein as storing excess Cu2+ and protecting other proteins from the effects of uncomplexed copper.

The effect of copper binding on the conformation of the prion protein was also investigated through very large scale molecular dynamics simulation. Our results show that copper binding alters the structure of the unfolded N-terminal domain, creating flexible turns in the octarepeat region that coordinates the copper ion. Furthermore, Cu binding increases the stability of the entire N-terminal domain, increasing its resistance to misfolding. The last results suggest that copper binding in the low concentration mode, which is the dominant one in vivo, delays the onset of prion diseases. The above results demonstrate the usefulness and capabilities of the KS/FDOF approach as a tool for investigating properties of solvated biomolecules and their reactions. This method should be particularly useful for studies of transition metal interactions with solvated biomolecules and of enzymatic reaction mechanisms, where an accurate quantum-mechanical description of fairly large solvated systems is needed.

References

[1] Tomasi J and Persico M. 1994. *Chemical Reviews* **94** 2027–2094.

[2] Rivail J L and Rinald D. 1995. *Liquid state quantum chemistry: computational applications of the polarizable continuum models* (World Scientific, Singapore).

[3] Cramer C J and Truhlar D G. 1996. *Continuum solvation models* (Kluwer, Dordrecht).

[4] Fattebert J and Gygi F. 2002. *Journal of Computational Chemistry* **23** 662–666.

[5] Begue D, Carbonniere P, Barone V, and Pouchan C. 2005. *Chemical Physics Letters* **416** 206–211.

[6] Guimarães L, Avelino de Abreu H, and Duarte H. 2007. *Chemical Physics* **333** 10–17.
[7] Bonifassi P, Ray P, and Leszczynski J. 2006. *Chemical Physics Letters* **431** 321–325.
[8] Zhou R and Berne B. 2002. *Proceedings of the National Academy of Sciences* **99** 12777–12782.
[9] Rhee Y M, Sorin E J, Jayachandran G, Lindahl E, and Pande V S. 2004. *Proc. National Acad. Sciences United States Am.* **101** 6456–6461.
[10] Warshel A and Levitt M. 1976. *J. Mol. Biol.* **102** 227–249.
[11] Singh U C and Kollmann P A. 1986. *J. Comput. Chem.* **7** 718–730.
[12] Field M J, Bash P A, and Karplus M. 1990. *J. Comput. Chem.* **11** 700–733.
[13] Kerdcharoen T and Morokuma K. 2002. *Chem. Phys. Lett.* **355** 257.
[14] Hodak M, Lu W, and Bernholc J. 2008. *J. Chem. Phys.* **128** 014101.
[15] Hodak M, Chisnell R, Lu W, and Bernholc J. 2009. *Proceedings of the National Academy of Sciences* **106** 11576.
[16] Prusiner S. 1997. *Science* **278** 245–251.
[17] Prusiner S. 1998. *Proc Natl Acad Sci USA* **95** 13363–13383.
[18] Baxa U, Cassese T, Kajava A, and Steven A. 2006. *Adv Protein Chem* **73** 125–80.
[19] Hornshaw M P, Mcdermott J R, Candy J M, and Lakey J H. 1995. *Biochem. Bioph. Res. Co.* **214** 993–999.
[20] Hornshaw M P, Mcdermott J R, and Candy J M. 1995. *Biochem. Bioph. Res. Co.* **207** 621–629.
[21] Brown D, Qin K, Herms J, Madlung A, Manson J, Strome R, Fraser P, Kruck T, vonBohlen A, SchulzSchaeffer W, Giese A, Westaway D, and Kretzschmar H. 1997. *Nature* **390** 684–687.
[22] Chattopadhyay M, Walter E, Newell D, Jackson P, Aronoff-Spencer E, Peisach J, Gerfen G, Bennett B, Antholine W, and Millhauser G. 2005. *J. Am. Chem. Soc.* **127** 12647–12656.
[23] Millhauser G. 2007. *Annu. Rev. Phys. Chem* **58** 299–320.
[24] Lee H, Lee C, and Parr R. 1991. *Phys. Rev. A* **44** 768.
[25] Soper A K. 2000. *Chem. Phys.* **258** 121.
[26] Wesolowski T and Warshel A. 1993. *J. Phys. C* **97** 8050.
[27] Vassallo N and Herms J. 2003. *J. Neurochem.* **86** 538–544.
[28] Inestrosa N, Cerpa W, and Varela-Nallar L. 2005. *IUBMB Life* **57** 645.
[29] Millhauser G. 2004. *Acc. Chem. Res* **37** 79–85.
[30] Whittal R, Ball H, Cohen F, Prusiner A, and Baldwin M. 2000. *Protein Sci.* **9** 332–343.
[31] Pauly P and Harris D. 1998. *J. Biol. Chem.* **273** 33107–33110.
[32] Aronoff-Spencer E, Burns C, Avdievich N, Gerfen G, Peisach J, Antholine W, Ball H, Cohen F, Prusiner S, and Millhauser G. 2000. *Biochem.* **39** 13760–13771.
[33] Burns C S, Aronoff-Spencer E, Legname G, Prusiner S B, Antholine W E, Gerfen G J, Peisach J, and Millhauser G L. 2003. *Biochem.* **42** 6794–6803.
[34] Bonomo R, Impellizzeri G, Pappalardo G, Rizzarelli E, and Tabbi G. 2000. *Chem.* **6** 4195–4202.
[35] Viles J, Cohen F, Prusiner S, Goodin D, Wright P, and Dyson H. 1999. *Proc. Natl. Acad. Sci. U.S.A.* **96** 2042–2047.
[36] Burns C S, Aronoff-Spencer E, Dunham C M, Lario P, Avdievich N I, Antholine W E, Olmstead M M, Vrielink A, Gerfen G J, Peisach J, Scott W G, and Millhauser G L. 2002. *Biochem.* **41** 3991–4001.
[37] Jackson G, Murray I, Hosszu L, Gibbs N, Waltho J, Clarke A, and Collinge J. 2001. *Proc. Natl. Acad. Sci. U.S.A.* **98** 8531–8535.
[38] Jones C E, Klewpatinond M, Abdelraheim S R, Brown D R, and Viles J H. 2005. *J. Mol. Biol.* **346** 1393–1407.
[39] Pushie M and Rauk A. 2003. *J. Biol. Inorg. Chem.* **8** 53–65.
[40] Wells M A, Jackson G S, Jones S, Hosszu L P, Craven C J, Clarke A R, Collinge J, and Waltho J P. 2006. *Biochem. J.* **399** 435–444.
[41] Klamt F, Dal-Pizzol F, da Frota M L C, Walz R, Andrades M E, da Silva E G, Brentani R R, Izquierdo I, and Moreira J C F. 2001. *Free Radical Bio. Med.* **30** 1137–1144.

[42] Rachidi W, Vilette D, Guiraud P, Arlotto M, Riondel J, Laude H, Lehmann S, and Favier A. 2003. *J. Bio. Chem.* **278** 9064–9072.
[43] Zeng F N, Watt N T, Walmsley A R, and Hooper N M. 2003. *J. Neurochem.* **84** 480–490.
[44] Wells M, Jelinska C, Hosszu L, Craven C, Clarke A, Collinge J, Waltho J, and Jackson G. 2006. *Biochem. J.* **400** 501–510.
[45] Walter E D, Chattopadhyay M, and Millhauser G L. 2006. *Biochem.* **45** 13083–13092.
[46] Schlitter J. 1993. *Chem. Phys. Lett.* **215**.
[47] Glykos N. 2006. *Journal of computational chemistry* **27** 1765.
[48] Phillips J C, Braun R, Wang W, Gumbart J, Tajkhorshid E, Villa E, Chipot C, Skeel R D, Kale L, and Schulten K. 2005. *J. Comput. Chem.* **26** 1781–1802.
[49] Linder M. 1991. *Biochem. Copp.* 73–134.
[50] Masuoka J, Hegenauer J, Van Dyke B, and Saltman P. 1993. *J. Bio. Chem.* **268** 21533–21537.
[51] Cox D, Pan J, and Singh R. 2006. *Biophysical journal* **91** 11–13.
[52] Govaerts C, Wille H, Prusiner S, and Cohen F. 2004. *Proceedings of the National Academy of Sciences of the United States of America* **101** 8342.
[53] Yang S, Levine H, Onuchic J, and Cox D. 2005. *The FASEB Journal* **19** 1778.